sustainability

MDPI

Article

Development of a High-Performance Electric Pressure Regulator Applied for Compressed-Natural-Gas-Fueled Vehicles

Nguyen Ba Hung [1,*] and Ocktaeck Lim [2,*]

1 School of Mechanical Engineering, Hanoi University of Science and Technology (HUST), 1 Dai Co Viet Road, Hai Ba Trung District, Hanoi 100000, Vietnam
2 School of Mechanical Engineering, University of Ulsan, Ulsan 44610, Korea
* Correspondence: hung.nguyenba1@hust.edu.vn (N.B.H.); otlim@ulsan.ac.kr (O.L.)

Received: 7 September 2020; Accepted: 22 September 2020; Published: 25 September 2020

check for updates

Abstract: A model-based study is carried out based on a combination of mathematical and Maxwell models to develop a high-performance electric pressure regulator utilized for compressed-natural-gas-fueled vehicles. To reduce computational cost, a symmetric two-direction model of the electric pressure regulator is established in Maxwell software, in which its material properties and dimension parameters are obtained on the base of specifications of a real electric pressure regulator. The output of simulating in Maxwell is the electromagnetic force, which is significantly improved when changing core shape in the various dimensions Δ1, Δ2, and Δ3. The optimal electromagnetic force is utilized for the mathematical models as an input variable to simulate the operational characteristics of the electric pressure regulator such as displacement and response time of plunger. The operational characteristics of the electric pressure regulator are examined under the influences of key parameters, including inlet gas pressure, diameter of orifice, and spring stiffness. By optimizing these key parameters, the simulated results in this study show that an electric pressure regulator with high performance can be obtained.

Keywords: pressure regulator; electromagnetic force; core shape; spring stiffness; orifice diameter

1. Introduction

An electric pressure regulator (EPR) is an energy-conversion device to control stable pressure for an injection system used gaseous fuel. The EPR can be combined with the hydrogen- and natural-gas-fueled injection systems to improve engine performance and reduce exhaust emission further [1–3]. Currently, studies relating to the EPR used for natural-gas-fueled injection systems are very few. Yamin and Hamdan [4] showed a gaseous regulator used for a spark ignition four-stroke engine fueled with hydrogen; however, they used a pressure regulator operated with the normal suction pressure that cannot be electrically controlled. Ehsan [5] investigated the effects of spark timing on the performance of a spark-ignition engine fueled with natural gas, in which a solenoid integrated pressure regulator was used to shut off the natural gas supplying the engine. Authors in reference [6] showed an EPR modeling used for a premixed compressed natural gas (CNG) engine; however, they did not mention solenoids in detail which strongly relates to the operation of an EPR.

The normal pressure regulators using mechanical mechanisms can limit the controlled pressure range because of their self-acting characteristics [7,8]. Thus, a new generation of pressure regulators like EPRs will be a potential candidate for replacing the normal pressure regulators, allowing for the flexible control of the gas pressure supplying the injector on the basis of the various working conditions of the internal combustion engine. The use of EPRs can help to control independently and precisely the injection pressure following the various working conditions to improve engine performance as well as exhaust emission.

A solenoid valve is used in the EPR structure, thus, the dynamic response, as well as the operating performance, of the EPR strongly depends on the opening and closing of the solenoid valve. Electromagnetic force is a decisional factor for the dynamic response of the solenoid valve, which is formed as the solenoid valve of EPR's supplied input current. The magnitude of the electromagnetic force is affected by the various parameters of the solenoid valve, including structural parameters (e.g., plunger shape, coil turns, coil location, etc.) and operating parameters (input current, voltage) [2,9,10]. Authors in reference [2] showed a simulation study to improve the electromagnetic force in a solenoid gas injector on the basis of influences of design parameters, including coil turns number, spring stiffness, and plunger mass. Liu et al. [9] indicated that by changing the structural parameters, including pole radius, yoke thickness of magnet, coil turns, air gap, and radius and thickness of armature, the electromagnetic force in a solenoid valve could be increased. Yoon et al. [10] optimized the plunger shape by using the finite element method combined with sequential quadratic programming to enhance the electromagnetic force. Cvetkovic et al. [11] investigated the effects of plunger pole shapes on the electromagnetic force of a fuel injector solenoid actuator using Maxwell software. Their simulation results showed that electromagnetic force could be increased when the plunger pole shapes were changed. Hung and Lim [12] presented a simulation study to improve the electromagnetic force of a solenoid injector, in which they changed the cross-sectional shape of the coil, thickness of the cut-off of the sleeve, and the relative position between the coil and plunger to obtain the highest electromagnetic force. The improvements of electromagnetic force based on the effects of structural parameters were also found in other studies [13–22]. The previous studies [2,9–22] provided useful information when improving electromagnetic force in a solenoid by optimizing design parameters such as plunger shape, plunger mass, coil shape, coil turns, coil location, air gap, pole radius, and yoke thickness of the magnet. However, core shape was rarely mentioned in the previous studies, which is considered one of the key parameters affecting electromagnetic force as well as the operating performance of a solenoid. The change of core shape can result in changing the magnetic field strength and flux line, thus, the electromagnetic force is also affected as a result.

The main purpose of this paper is to improve the electromagnetic force of a solenoid used for an EPR using a model-based study under the influence of the core shape. Mathematical models are used to describe the operation of the EPR including electrical and mechanical models. In addition, to simulate electromagnetic force, a two-dimensional (2D) model of the EPR is established in Maxwell, in which the 2D model has a symmetric type to save the computational cost. Material features, dimensional parameters, and operating conditions of the EPR 2D model are selected based on specifications of a real EPR. In the 2D model-based study, electromagnetic force is examined based on the change of core shape. The highest electromagnetic force obtained by optimizing the core shape is imported into the mathematical models to simulate the dynamic response of the EPR. The effects of gas pressure in inlet, spring stiffness, and orifice diameter on the dynamic response of the EPR are investigated.

2. Mathematical Models

An EPR utilizes a solenoid valve to open and close the inlet gas port, which includes two main parts: the mechanical part (e.g., spring, plunger) and the electrical part (e.g., coil). When the coil of an EPR is provided the input current, the plunger moves in upward to open the inlet gas port while the spring is compressed. Afterward, if the supply of input current is stopped, the plunger will be pushed back to close the inlet gas port due to the spring elastic force. In order to describe the operation of the EPR, mathematical models are established, including mechanical and electrical models.

2.1. Mechanical Model

In order to describe the mechanical operation of an EPR, an operating model and a force analysis model are shown in Figure 1a,b, respectively. When the EPR is activated by input current, the plunger is moved in upward under the support of electromagnetic force and gas force. However, its motion is also affected by resistance forces such as gravitational force and elastic force caused by plunger mass and spring, respectively. Table 1 shows the specifications of an EPR, in which the EPR is designed with a range of inlet maximum gas pressure from 20 bar to 30 bar. The plunger motion obeys the second law of Newton, as described by the following equations:

$$\sum F = m_{pr}\frac{d^2x_{pr}}{dt^2} \quad (1)$$

$$F_{er} - F_{sr} - F_{dr} + F_p - F_{gr} = m_{pr}\frac{d^2x_{pr}}{dt^2} \quad (2)$$

$$F_{er} - k_r(x+\Delta) - b_r\frac{dx_{pr}}{dt} + P_{in}S_o - m_{pr}g = m_{pr}\frac{d^2x_{pr}}{dt^2} \quad (3)$$

where, F_{er} is electromagnetic force, F_{sr} is spring force, F_{dr} is damping force, F_{gr} is gravitational force, F_p is pressure force, k_r is spring stiffness, Δ is initial compression, m_{pr} is plunger mass, P_{in} is inlet pressure, S_o is orifice cross-sectional area, and x_{pr} is plunger displacement of the EPR.

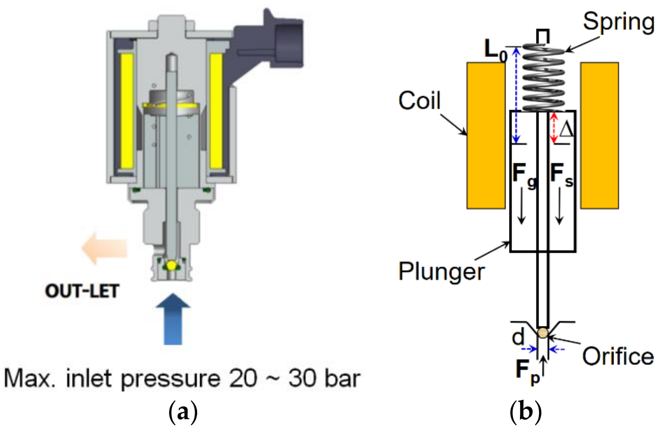

Figure 1. Electric pressure regulator (EPR) with (**a**) operating model and (**b**) force analysis model.

Table 1. EPR specification.

Parameters	Value
Input current (A)	2.9
Resistance of the coil (Ω)	4.1
Coil turns number	600
Inlet maximum gas pressure (bar)	20–30
Mass of plunger (g)	31
Spring free length (mm)	17
Spring initial compression (mm)	9.7

2.2. Electrical Model

Electromagnetic force appears when the coil of an EPR is provided by input voltage, which helps the plunger to move in upward, as shown in Figure 1b. The input voltage is described through an equation showing its relationship with coil resistance, current, and total flux of winding [2]:

$$v_{0r} = R_r i_r + \frac{d\lambda_r}{dt} \quad (4)$$

where, λ_r is the total flux in the EPR, v_{or} is voltage providing to the EPR, i_r is current in the coil of the EPR, R_r is coil resistance of the EPR.

λ_r is also described as a function of current, which is presented by:

$$\lambda_r = L(x_{pr})i_r \quad (5)$$

where $L(x_{pr})$ is inductance of the EPR.

The voltage and current providing to the coil of the EPR are derived by combining Equations (4) and (5):

$$v_{0r} = R_r i_r + L(x_{pr})\frac{di_r}{dt} + i_r\frac{dL(x_{pr})}{dx_{pr}}\frac{dx_{pr}}{dt} \quad (6)$$

$$\frac{di_r}{dt} = \frac{1}{L(x_{pr})}\left[v_{0r} - R_r i_r - i_r\frac{dL(x_{pr})}{dx_{pr}}\frac{dx_{pr}}{dt}\right] \quad (7)$$

The current in Equation (7) is used as a variable to calculate the electromagnetic force which is presented by the following equations [23]:

$$W'_m(i_r, x_{pr}) = \int_0^{i_r} \lambda(i_r, x_{pr})di_r = \int_0^{i_r} L(x_{pr}).i_r di_r = \frac{1}{2}i_r^2.L(x_{pr}) \quad (8)$$

$$F_{er} = \frac{\partial W'_m(i_r, x_{pr})}{\partial x_{pr}} = \frac{1}{2}i_r^2.\frac{dL(x_{pr})}{dx_{pr}} \quad (9)$$

where $W'_m(i_r, x_{pr})$ is co-energy [23], which is a function of the inductance and current in the coil.

The inductance of the EPR is defined by [24]:

$$L(x_{pr}) = \frac{N_r^2}{\sum_1^n \Re_{ri}} \quad (10)$$

where $\sum_1^n \Re_{ri}$ is the total reluctance of the EPR and N_r is coil turns number.

3. EPR Model in Maxwell

A 2D (two dimensional) drawing of the EPR is produced by computer-aided design (CAD) software. Afterward, this 2D drawing of the EPR is imported into Maxwell software to simulate the electromagnetic force. A 2D model of the EPR is created in Maxwell along with its specifications, which is based on operating and structure parameters of a real EPR. To reduce computation cost, the 2D model of the EPR in Maxwell is created with a symmetric type as presented in Figure 2.

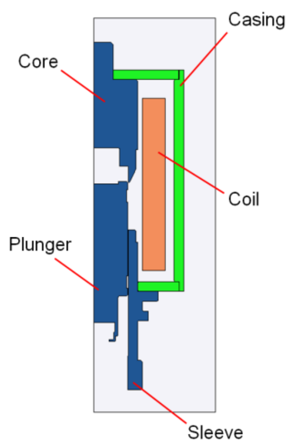

Figure 2. Symmetric model of the EPR in Maxwell.

The specifications of the EPR such as resistance of the coil, coil turns number, and input current are utilized as initial parameters for the 2D model of the EPR in Maxwell. Material features of components of the EPR are also used as initial parameters to model the electromagnetic force and magnetic characteristics of the EPR. The materials are selected based on materials of real components, which are presented in Table 2.

Table 2. Materials of components in EPR.

Components	Material Type	Material Name
Coil	Copper	Copper
Plunger	Stainless steel	S416
Sleeve	Stainless steel	S416
Casing	Stainless steel	S430
Core	Stainless steel	S416

4. Effecting Flowchart

Core shape is considered to be a key parameter affecting the electromagnetic force of the EPR, which is not mentioned in the previous studies. In this study, to observe how the electromagnetic force is varied and obtain optimal value, the core shape of EPR is changed based on the change of its dimensions. In addition, defining the required spring stiffness is needed to ensure that the inlet hole of the EPR is closed by spring force acting on the plunger at a static state without electromagnetic force. Based on the influences of inlet gas pressure and diameter of the orifice, the spring stiffness is suitably designed to ensure the closing inlet hole of the EPR mentioned above. The required spring stiffness and the electromagnetic force optimized by changing the core shape are used as input parameters for the mathematical model to calculate and analyze the dynamic response of the EPR. A flowchart is made to see how these parameters affect the operating characteristics of the EPR, which is described in Figure 3.

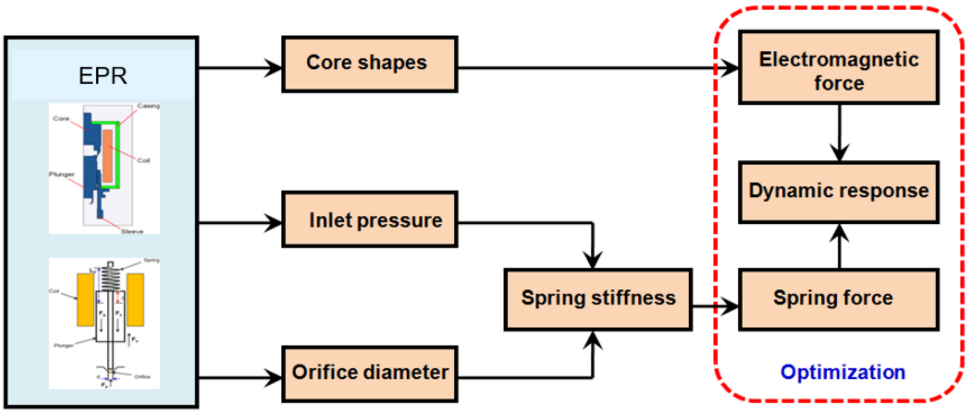

Figure 3. A flowchart for analyzing the dynamic response of the EPR based on influences of input parameters.

5. Simulation Results

5.1. Analysis and Optimization for Electromagnetic Force

The electromagnetic force is analyzed and optimized based on the effects of core shape. The core shape is varied based on its dimensions, which is depicted by dimension parameters $\Delta 1$, $\Delta 2$, and $\Delta 3$, as shown in Figure 4. The core is designed in a special shape to increase the electromagnetic force, which is not mentioned in the previous studies. The dimensions $\Delta 1$, $\Delta 2$, and $\Delta 3$ are considered to be key parameters related to changing the flux lines on the core, thus, they affect the electromagnetic force. This section examines the influences of core shape for the electromagnetic force based on the change of $\Delta 1$, $\Delta 2$, and $\Delta 3$.

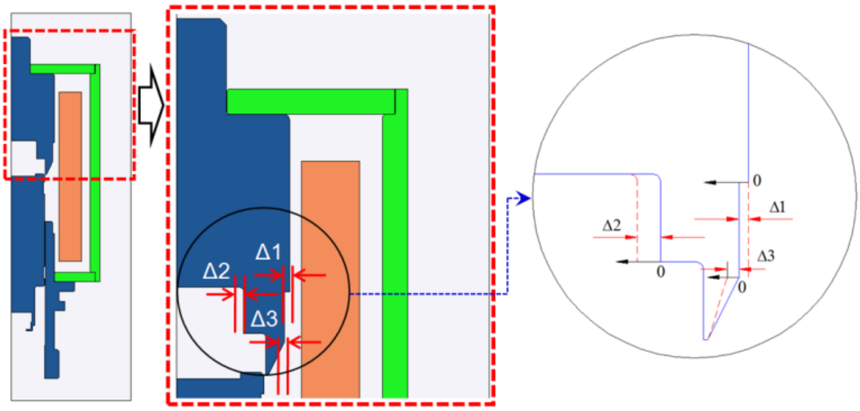

Figure 4. The change of core shape in dimension parameters.

5.1.1. The Influences of Δ1

Figure 5 shows influences of Δ1 for electromagnetic force versus stroke of the plunger, in which the value of Δ1 is changed from 0 mm to 0.8 mm. The initial parameters, including resistance of the coil, input current, and coil turns number are respectively kept at 4.1 Ω, 2.9 A, and 600. When Δ1 is increased, the electromagnetic force is decreased, as observed in Figure 5. Reduced magnetic flux line on the core due to the increase of Δ1 can be a cause of this phenomenon, which results in the reduction of the electromagnetic force. As can be seen in Figure 5, the values of electromagnetic force at Δ1 = 0 mm are almost higher than that of Δ1 = 0.4 mm and Δ1 = 0.8 mm, thus, it can be selected as an optimal value among the various values of Δ1.

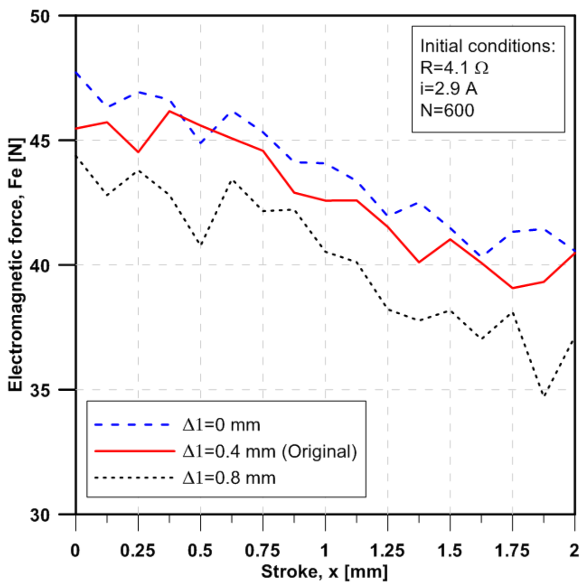

Figure 5. The influences of Δ1 on electromagnetic force.

5.1.2. The Influences of Δ2

The influences of Δ2 for electromagnetic force are shown in Figure 6, in which the value of Δ2 is changed from 0 mm to 2 mm. The initial conditions—input current, resistance of the coil, and coil turns number—are kept at 2.9 A, 4.1 Ω, and 600, respectively. The electromagnetic force is increased when Δ2 is increased, which is observed in Figure 6. The increase of Δ2 leads to improving the electromagnetic force, which is clearly seen when Δ2 is changed from 0 mm to 1 mm. The electromagnetic force has a slightly increased trend as Δ2 continues to increase to 2 mm. This phenomenon can be explained that the magnetic flux line towards the plunger increases and then obtains a saturation state because Δ2 is increased while Δ3 is not changed.

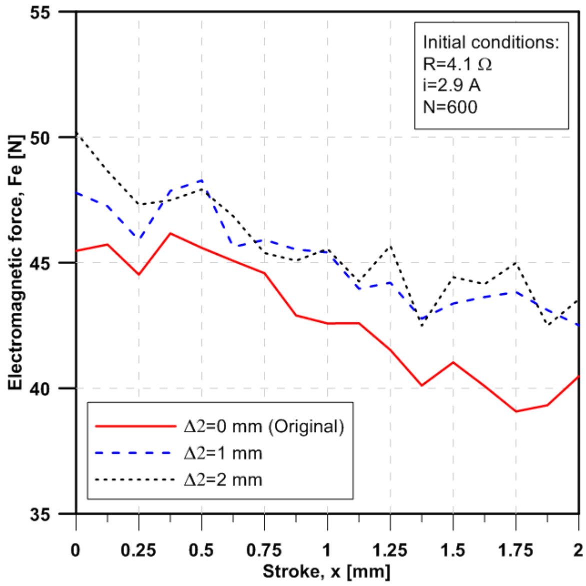

Figure 6. The influences of Δ2 on electromagnetic force.

5.1.3. The Influences of Δ3

Figure 7 shows the influences of Δ3 for electromagnetic force, in which the value of Δ3 is changed from 0 mm to 1 mm. The initial conditions including resistance of the coil, coil turns number, and input current are retained constant. The change of Δ3 leads to different changing tendencies of the electromagnetic force, as observed in Figure 7.

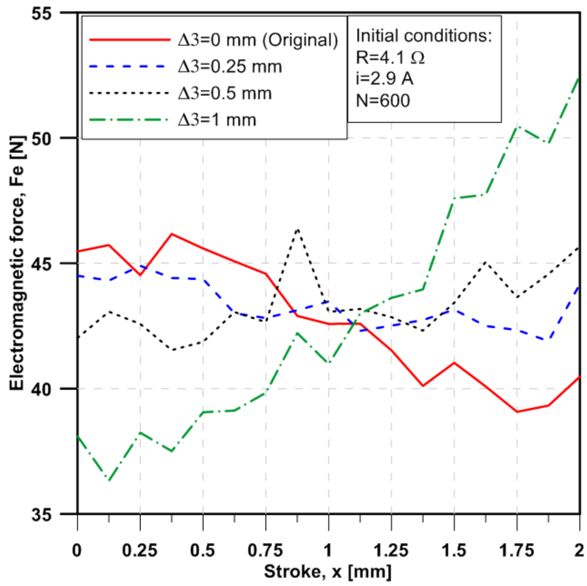

Figure 7. The influences of Δ3 on electromagnetic force.

The electromagnetic force has reduced tendency as Δ3 is changed from 0 mm to 1 mm and the stroke of the plunger is increased from 0 mm to 1 mm. Nevertheless, the electromagnetic force then increases again when the stroke of the plunger continues to increase from 1 mm to 2 mm, which shows an opposite tendency when compared with the electromagnetic force of the previous stage of plunger stroke (0 mm to 1 mm). The increase of Δ3 results in increasing the slope angle of the core, which can orient better the magnetic flux lines toward the plunger.

5.1.4. Optimization of Electromagnetic Force

Based on the results obtained in the prior sections, the values of 0 mm, 2 mm, and 0.25 mm can be selected as optimal values for Δ1, Δ2, Δ3, respectively. To make an optimal shape of the core, the parameters Δ1, Δ2, and Δ3 are combined. In this way, the electromagnetic force of the EPR can be significantly improved. Figure 8 shows a comparison between the electromagnetic force of the original and developed versions of EPR under the combined influences of Δ1, Δ2, and Δ3.

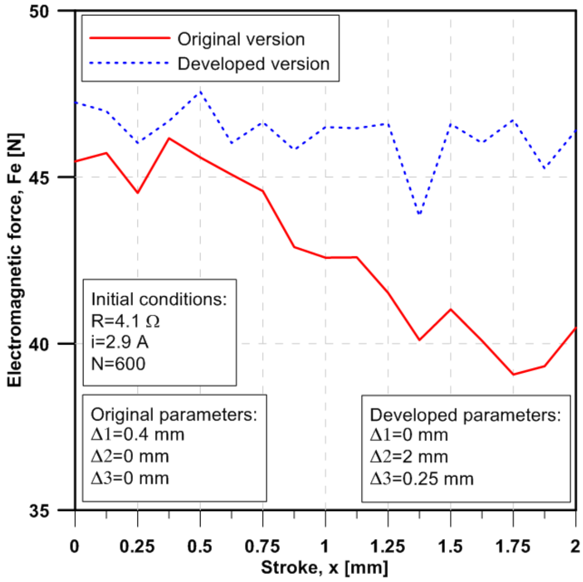

Figure 8. The combined influence of Δ1, Δ2, and Δ3 on electromagnetic force.

By selecting the optimal values of Δ1, Δ2, and Δ3, the electromagnetic force of the developed EPR is considerably improved when compared to the electromagnetic force of the original version of the EPR, as observed in Figure 8. It can be seen that the improvement of electromagnetic force at a plunger stroke of 1.75 mm is highest (16.4 %). In addition, the electromagnetic force profile tends to be horizontal, which shows a high operating performance of the developed EPR.

Figure 9 shows a comparison in magnetic field strength between the original version and developed version of the EPR, in which the magnetic field strength is obtained at the various plunger strokes. For the developed version, the values of the magnetic field strength concentrated between the plunger and core have an increasing trend when compared with the original version, which can lead to improving electromagnetic force as presented in Figure 8.

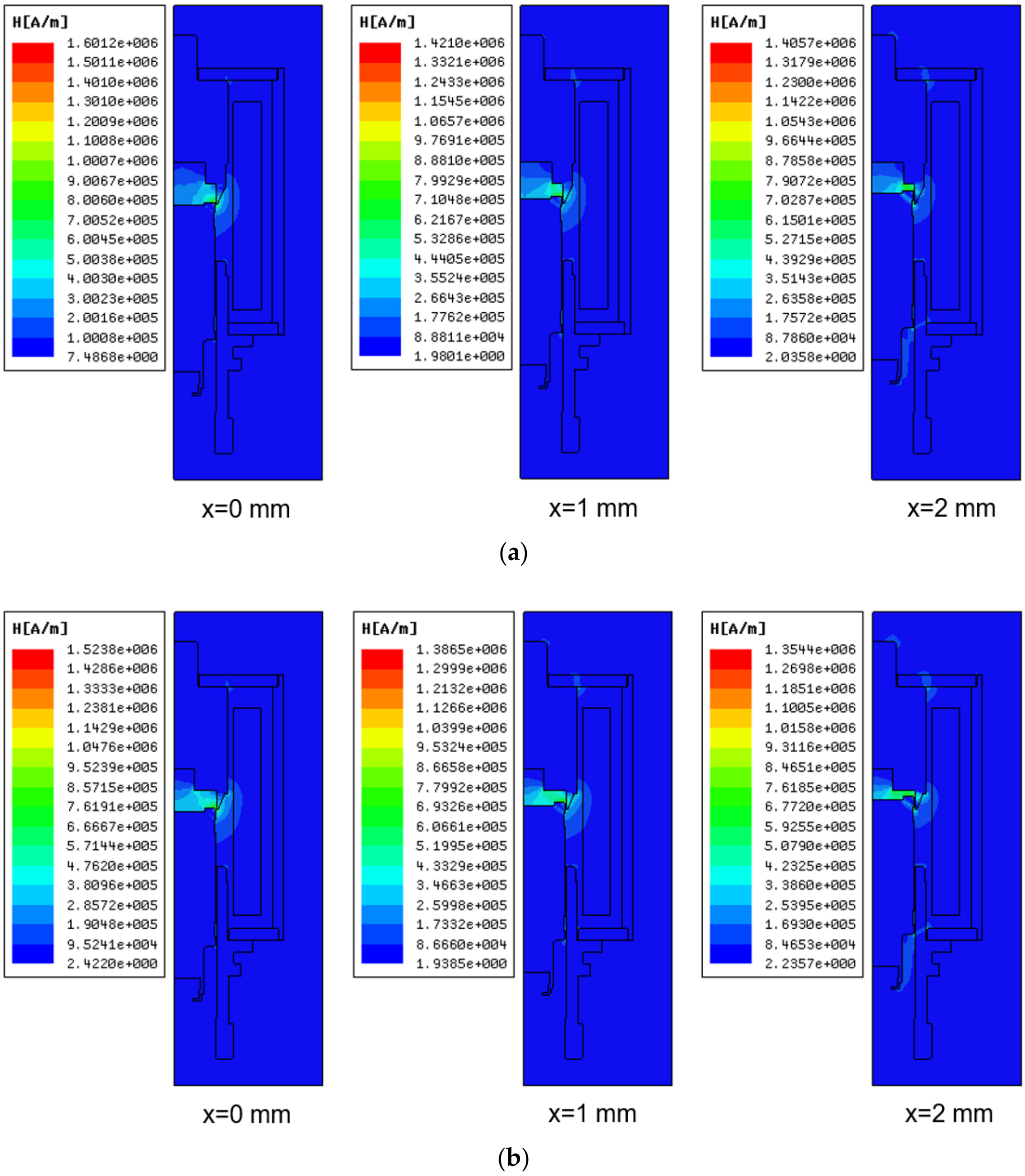

Figure 9. Magnetic field strength of (**a**) original version and (**b**) developed version.

5.2. Requirement for Spring Stiffness and Spring Force

When the EPR is not operated (static state), the plunger closes the inlet gate of the EPR through the spring force. The plunger can be pushed by gas pressure force and the inlet gate of the EPR is opened if spring stiffness is not high enough. The gas pressure force at the inlet gate of the EPR depends on orifice diameter and inlet pressure. Thus, it is needed to define requirements for spring stiffness as well as spring force following the orifice diameter and inlet pressure to make certain that the plunger can close the inlet gate in the static state of the EPR. The requirements for spring stiffness as well as spring force are defined based on the influences of orifice diameter and inlet gas pressure as shown in Figure 10. The orifice diameter is changed from 2.5 mm to 3.5 mm, and the inlet gas pressure is varied at 20 bar, 25 bar, and 30 bar. When the orifice diameter is increased while the inlet gas pressure is retained at 20 bar, the spring force and stiffness of the spring increased by 49.7%. In addition, the spring force and stiffness of spring increased by 34% when increasing the inlet gas pressure, as shown in Figure 10. The optimal electromagnetic force obtained previously along with the values of spring stiffness obtained in Figure 10 are utilized as inputs to investigate the influences of inlet gas pressure and orifice diameter on response characteristics of the EPR.

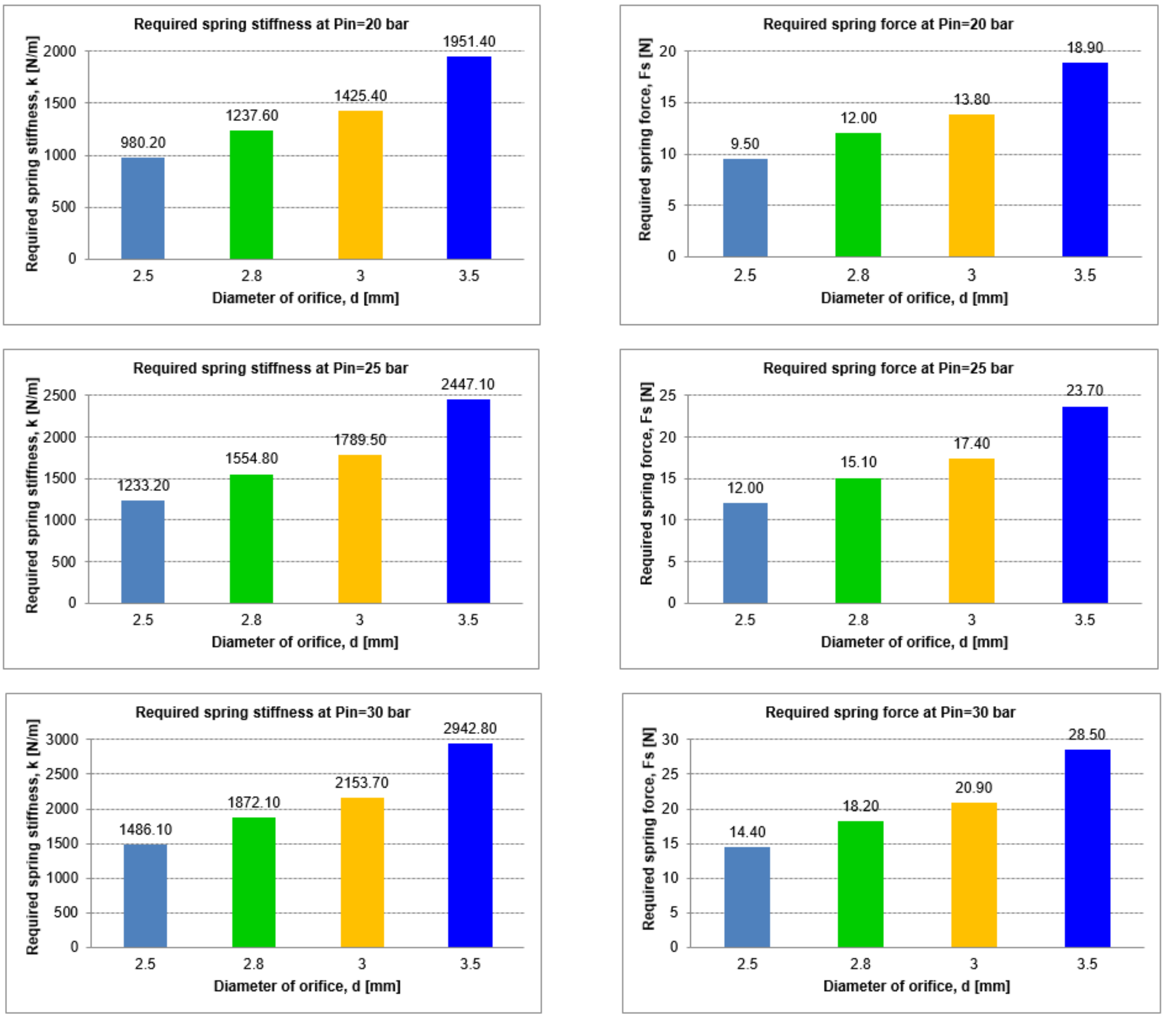

Figure 10. Requirements for spring force and stiffness of spring based on the influences of orifice diameter and inlet gas pressure.

5.3. Characteristics of Dynamic Response

In a transient state, characteristics of dynamic response depend on design parameters as well as electromagnetic force, which play a key role in designing a high-performance EPR. The effects of inlet gas pressure and orifice diameter on the displacement of the plunger are shown in Figures 11–13. The initial conditions including input current, resistance of the coil, coil turns number, input voltage duration, and spring stiffness are retained at 2.9 A, 4.1 Ω, 600, 5 ms, and 2942.8 N/m, respectively. When the diameter of the orifice is increased, the plunger displacement reaches the maximum value faster, as observed by an enlarged picture in Figure 11. By increasing inlet gas pressures, this tendency is also observed, as shown in Figures 12 and 13. This can be explained through the increase of gas pressure force due to the increased orifice diameter. In addition, when the gas pressure at the inlet gate is increased, the plunger displacement reaches the maximum value faster because the gas pressure force is increased as the inlet gas pressure is increased.

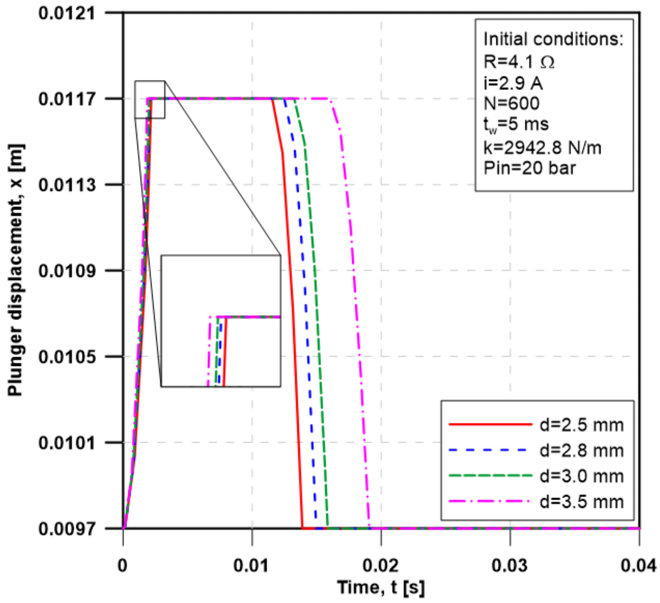

Figure 11. Displacement of the plunger under the effect of orifice diameter as inlet pressure is kept at 20 bar.

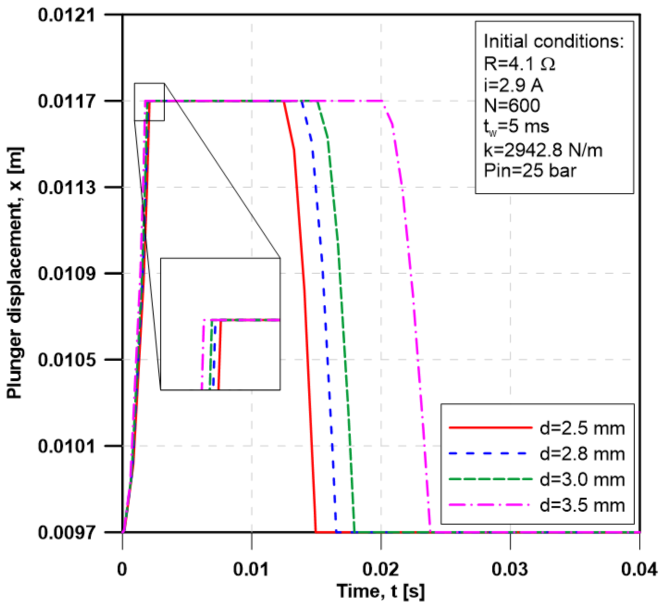

Figure 12. Displacement of the plunger under the effect of orifice diameter as inlet pressure is kept at 25 bar.

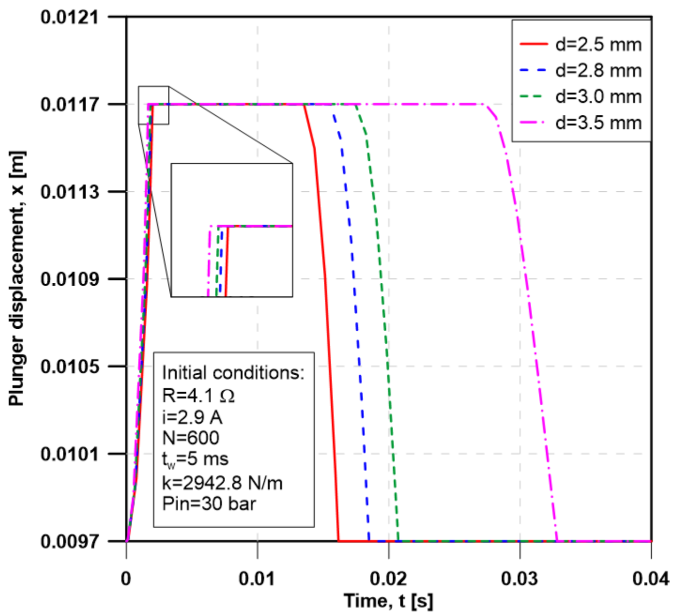

Figure 13. Displacement of the plunger under the effect of orifice diameter as inlet pressure is kept at 30 bar.

When the supply input voltage to the EPR is stopped, the plunger is pushed down by the elastic spring force to close the inlet gate. The plunger displacement in this stage is strongly affected by the spring elastic force as well as spring stiffness. The displacement of the plunger is decreased to the initial position earlier as the diameter of the orifice is reduced, as observed in Figure 11. This can be explained by the influences of the elastic spring force and gas pressure force for the motion of the plunger during the close stroke. When the diameter of the orifice is reduced, the gas pressure force is also reduced accordingly, thus, the difference between the elastic spring force and the gas pressure force is increased. As the result, the displacement of the plunger decreases earlier during the close stroke when the diameter of the orifice is reduced. It can be seen that the increased orifice diameter has a benefit for the open stroke, but it is also a disadvantage for the close stroke of the plunger in the EPR.

The influences of inlet gas pressure and orifice diameter on the response time of open and close processes of EPR are presented in Figures 14 and 15, respectively. The simulation results in Figure 14 show that by increasing the diameter of the orifice, the response time of the open process is decreased. In addition, increasing the inlet gas pressure has also a benefit for reducing the response time of the open process. It can be seen that when the inlet gas pressure and orifice diameter are 30 bar and 3.5 mm, respectively, the value of open response time is smallest (1.66 ms), as shown in Figure 14. Figure 15 shows the influences of inlet gas pressure and orifice diameter on the response time of the close process of the EPR. As shown in Figure 15, the response time of the close process is higher than that of the open process at the same values of inlet gas pressure and orifice diameter, which can be explained by the resistance force for the plunger motion due to the inlet gas pressure. Unlike the trend of response time in the open process, when the diameter of the orifice and inlet gas pressure are increased, the response time of the close process has an increasing trend due to the increased gas pressure force. Therefore, a suitable selection of inlet gas pressure and the diameter of the orifice can optimize the response time of open and close processes of the EPR.

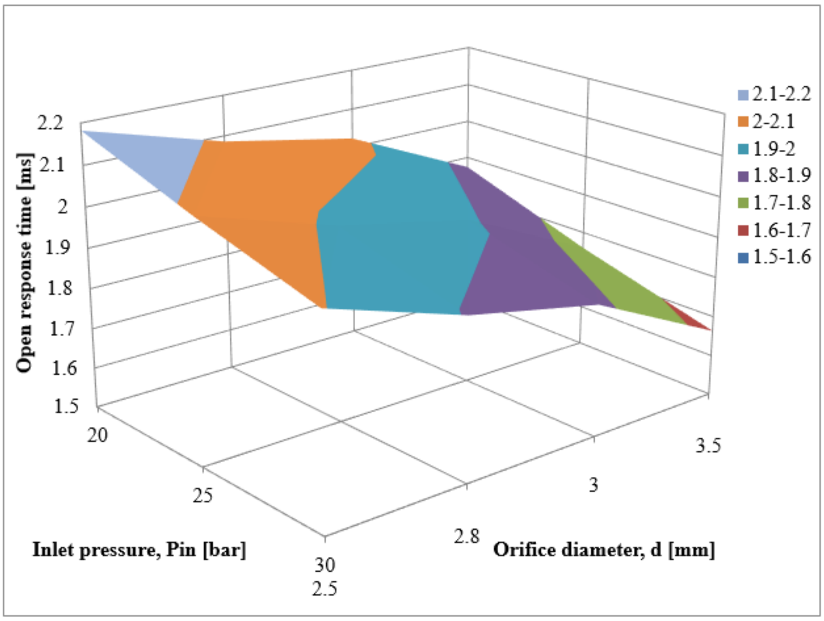

Figure 14. The influences of inlet gas pressure and orifice diameter for open response time.

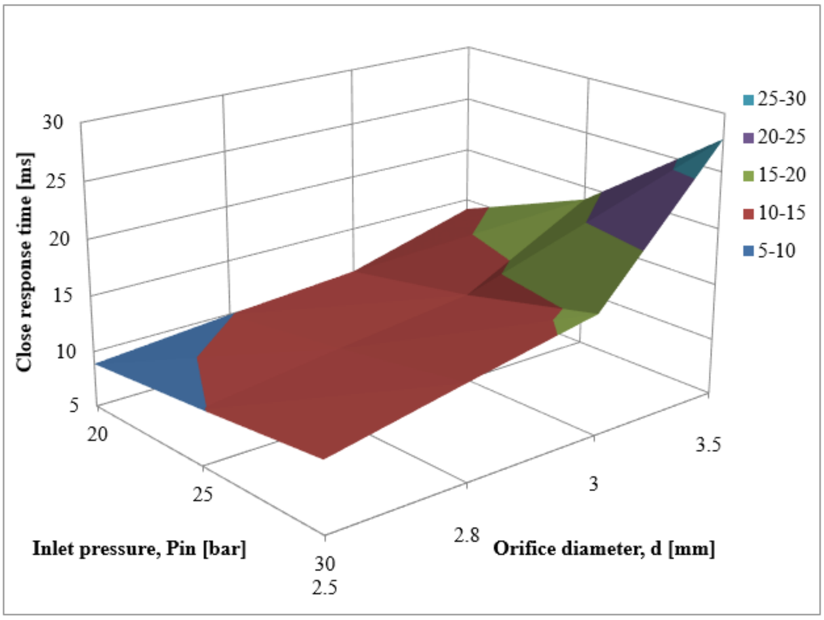

Figure 15. The influences of inlet gas pressure and orifice diameter for close response time.

6. Conclusions

The operation of the EPR has been modeled by using a combination of mathematical and Maxwell models. A developed study was conducted to predict the influences of the core shape for the electromagnetic force, in which new shapes of the core were proposed by changing its dimensional parameters, including Δ1, Δ2, and Δ3. This study indicated that the change of core shape through the variation of Δ1, Δ2, and Δ3 considerably improved the electromagnetic force of the EPR. The simulation results showed that when Δ1, Δ2, and Δ3 were varied at 0 mm, 2 mm, and 0.25 mm, respectively, the electromagnetic force was optimized. The response characteristics of the EPR were then investigated using the electromagnetic force optimized before. The influences of EPR design parameters, including required spring stiffness, inlet gas pressure, and orifice diameter, on the response characteristics of the EPR were investigated. When the inlet gas pressure and orifice diameter, respectively, were increased to 30 bar and 3.5 mm, the open response time was significantly reduced, while the close response time was considerably increased due to the influence of the increased inlet gas pressure. By selecting the design parameters appropriately, the open and close response time of the EPR could be optimized. The model-based study could be beneficial guidelines to design and develop an EPR with high operating performance, applied for CNG-fueled vehicles to increase efficiency and reduce exhaust emission.

Author Contributions: Conceptualization, N.B.H. and O.L.; methodology, N.B.H.; software, N.B.H. and O.L.; validation, N.B.H. and O.L.; formal analysis, N.B.H.; investigation, N.B.H.; resources, N.B.H.; data curation, N.B.H.; writing—original draft preparation, N.B.H. and O.L.; writing—review and editing, N.B.H. and O.L.; visualization, N.B.H.; supervision, N.B.H. and O.L.; project administration, N.B.H.; funding acquisition, N.B.H. All authors have read and agreed to the published version of the manuscript.

Funding: This research received no external funding.

Acknowledgments: This research is funded by the Hanoi University of Science and Technology (HUST) under project number T2020-TT-007.

Conflicts of Interest: The authors declare no conflict of interest.

References

1. Ding, L.; Wu, J. Innovation ecosystem of CNG vehicles: A case study of its cultivation and characteristics in Sichuan, China. *Sustainability* **2018**, *10*, 39. [CrossRef]
2. Hung, N.B.; Lim, O.T.; Yoon, S.J. Effects of structural parameters on operating characteristics of a solenoid injector. *Energy Procedia* **2017**, *105*, 1771–1775. [CrossRef]
3. Wang, X.; Zhang, H.; Yao, B.; Lei, Y.; Sun, X.; Wang, D.; Ge, Y. Experimental study on factors affecting lean combustion limit of S.I engine fueled with compressed natural gas and hydrogen blends. *Energy* **2012**, *38*, 58–65. [CrossRef]
4. Yamin, J.A.; Hamdan, M.A. The performance of hydrogen-powered 4-stroke SI engine using locally designed fuel regulator. *J. Braz. Soc. Mech. Sci. Eng.* **2010**, *32*, 195–199. [CrossRef]
5. Ehsan, M. Effect of spark advance on a gas run automotive spark ignition engine. *J. Chem. Eng.* **2006**, *24*, 42–49. [CrossRef]
6. Liu, Y.; Li, J.; Qu, D. Modeling and analysis of electronic pressure regulator of premixed CNG engine. *IOP Conf. Ser. Mater. Sci. Eng.* **2018**, *382*, 1–7. [CrossRef]
7. Ramzan, M.; Maqsood, A. Dynamic modeling and analysis of a high pressure regulator. *Math. Probl. Eng.* **2016**, *2016*, 1–8. [CrossRef]
8. Patil, M.G.; Barjibhe, R.B. Flow analysis of gas pressure regulator by numerical & experimental method. *Int. Res. J. Eng. Technol.* **2018**, *5*, 747–752.
9. Liu, P.; Fan, L.; Hayat, Q.; Xu, D.; Ma, X.; Song, E. Research on key factors and their interaction effects of electromagnetic force of high-speed solenoid valve. *Sci. World J.* **2014**, *2014*, 1–13. [CrossRef]
10. Yoon, S.B.; Hur, J.; Chun, Y.D.; Hyun, D.S. Shape optimization of solenoid actuator using the finite element method and numerical optimization technique. *Sci. World J.* **2014**, *2014*, 1–13.
11. Cvetkovic, D.; Cosic, I.; Subic, A. Improved performance of the electromagnetic fuel injector solenoid actuator using a modelling approach. *Int. J. Appl. Electromagn. Mech.* **2008**, *27*, 251–273. [CrossRef]
12. Hung, N.B.; Lim, O.T. Improvement of electromagnetic force and dynamic response of a solenoid injector based on the effects of key parameters. *Int. J. Automot. Technol.* **2019**, *20*, 949–960. [CrossRef]
13. Yin, L.; Wu, C. The characteristic analysis of the electromagnetic valve in opening and closing process for the gas injection system. *J. Electromagn. Anal. Appl.* **2016**, *8*, 152–159. [CrossRef]
14. Yang, M.; Zhang, J.; Xu, B. Experimental study and simulation analysis on electromagnetic characteristics and dynamic response of a new miniature digital valve. *Adv. Mater. Sci. Eng.* **2018**, *2018*, 1–8. [CrossRef]
15. Zhao, J.; Fan, L.; Liu, P.; Grekhov, L.; Ma, X.; Song, E. Investigation on electromagnetic models of high-speed solenoid valve for common rail injector. *Math. Probl. Eng.* **2017**, *2017*, 1–10. [CrossRef]
16. Sun, Z.Y.; Li, G.X.; Wang, L.; Wang, W.H.; Gao, Q.X.; Wang, J. Effects of structure parameters on the static electromagnetic characteristics of solenoid valve for an electronic unit pump. *Energy Convers. Manag.* **2016**, *113*, 119–130. [CrossRef]

17. De, X.; Zi, F.H.; Peng, L.; Wei, Z.; Yun, F.L. Electromagnetic force of high-speed solenoid valve based on correlation analysis. *Int. J. Smart Sens. Intell. Syst.* **2015**, *8*, 2267–2285. [CrossRef]
18. Shin, Y.; Lee, S.; Choi, C.; Kim, J. Shape optimization to minimize the response time of direct-acting solenoid valve. *J. Magn.* **2015**, *20*, 193–200. [CrossRef]
19. Xu, X.; Han, X.; Liu, Y.; Liu, Y.; Liu, Y. Modeling and dynamic analysis on the direct operating solenoid valve for improving the performance of the shifting control system. *Appl. Sci.* **2017**, *7*, 1266. [CrossRef]
20. Song, C.W.; Lee, S.Y. Design of a solenoid actuator with a magnetic plunger for miniaturized segment robots. *Appl. Sci.* **2015**, *5*, 595–607. [CrossRef]
21. Lee, H.R.; Ahn, J.H.; Kim, H.Y. Design of a solenoid actuator for a cylinder valve in a fuel cell vehicle. *Appl. Sci.* **2016**, *6*, 288. [CrossRef]
22. Hung, N.B.; Lim, O.T. A simulation and experimental study on the operating characteristics of a solenoid gas injector. *Adv. Mech. Eng.* **2019**, *11*, 1–14. [CrossRef]
23. Woodson, H.H.; Melcher, J.R. *Electromechanical Dynamics*; John Wiley & Sons Inc.: New York, NY, USA, 1968.
24. Giurgiutiu, V.; Lysheyski, S.E. *Micromechatronics: Modeling, Analysis, and Design with MATLAB*, 2nd ed.; CRC Press: Boca Raton, FL, USA, 2009.